Rhombohedral Structure of Highly Ordered and Oriented Self-Assembled Nanoporous Silica Thin Films

Brian W. Eggiman, Michael P. Tate, and Hugh W. Hillhouse*

School of Chemical Engineering, Purdue University, 480 Stadium Mall Drive, West Lafayette, Indiana 47907-2050

Received September 15, 2005. Revised Manuscript Received December 2, 2005

Nanoporous silica films have been synthesized by self-assembly on substrates by dip-coating from a combined solution of aged silica oligomers and poly(ethylene oxide)$_{20}$−poly(propylene oxide)$_{70}$−poly-(ethylene oxides)$_{20}$ triblock copolymer (Pluronic P123) in ethanol and water. The films are indexed with the rhombohedral space group $R\bar{3}m$ and are oriented through the thickness of the film with the (111) axis perpendicular to the substrate. Sixfold symmetry perpendicular to the substrate is directly observed by high-resolution top-view field emission scanning electron microscopy over the entire substrate. The films have domains that sample many orientations in the plane of the substrate resulting in a reciprocal space composed of rings. These rings are directly observed by collecting small-angle X-ray scattering data at many angles of incidence from transmission (beam perpendicular to the substrate) all the way down to the grazing angle of incidence. At each rotation, the Bragg spot location in the two-dimensional pattern is quantitatively predicted by an $R\bar{3}m$ unit cell with lattice constants $a = 112$ Å and $\alpha = 86°$. On the basis of these lattice constants, it is conjectured that the rhombohedral structure results from a uniaxial contraction of a (111) oriented film of self-assembled aggregates ordered on a face-centered cubic lattice. The film structure and orientation reported here differ from previous reports of cubic, or distorted cubic, nanoporous films synthesized with P123 and F127 and are expected to be important steps in controlling structure and accessibility in nanoporous films.

1. Introduction

Ordered nanoporous inorganic materials formed via self-assembly of templating molecules[1−4] are unique in that they have very monodisperse pore size and well-defined pore shape/connectivity in addition to their high surface area. These materials have many exciting applications in nanoscale casting, catalysis, and adsorption and have recently been reviewed by several groups.[5−11] Thin film morphologies have potential applications as low dielectric constant films,[12,13] low refractive index films,[14−16] hydrogen sensors,[17] nanostructured magnetic materials,[18] photomodulated mass-transport layers,[19] nanostructured solar cells,[20] and nanostructured thermoelectrics.[21] For most of these applications, pore connectivity, mass transport, ion transport, and/or electron transport are key factors to control in the engineering of new devices. In addition, for applications such as thermoelectrics, the small pores size afforded by this synthesis route (2−10 nm) make these films better candidates for generating nanostructured materials that exhibit quantum confinement when compared to other film synthesis methods[22−24] that typically yield larger pore sizes (>10 nm). Thus, one of the

* Corresponding author. E-mail: hugh@purdue.edu.

(1) Kresge, C. T.; Leonowicz, M. E.; Roth, W. J.; Vartuli, J. C.; Beck, J. S. *Nature* **1992**, *359*, 710−712.
(2) Monnier, A.; Schuth, F.; Huo, Q.; Kumar, D.; Margolese, D.; Maxwell, R. S.; Stucky, G. D.; Krishnamurty, M.; Petroff, P.; Firouzi, A.; Janicke, M.; Chmelka, B. F. *Science* **1993**, *261*, 1299−1303.
(3) Huo, Q.; Margolese, D.; Cielsa, U.; Feng, P.; Gler, T. E.; Sieger, P.; Leon, R.; Petroff, P. M.; Schuth, F.; Stucky, G. D. *Nature* **1994**, *368*, 317−321.
(4) Firouzi, A.; Kumar, D.; Bull, L. M.; Besier, T.; Sieger, P.; Huo, Q.; Walker, S. A.; Zasadzinski, J. A.; Glinka, C.; Nicol, J.; Margolese, D.; Stucky, G. D.; Chmelka, B. F. *Science* **1995**, *267*, 1138−1143.
(5) Yang, H. F.; Zhao, D. Y. *J. Mater. Chem.* **2005**, *15*, 1217−1231.
(6) Taguchi, A.; Schuth, F. *Microporous Mesoporous Mater.* **2005**, *77*, 1−45.
(7) Soler-Illia, G.; Crepaldi, E. L.; Grosso, D.; Sanchez, C. *Curr. Opin. Colloid Interface Sci.* **2003**, *8*, 109−126.
(8) Stein, A. *Adv. Mater.* **2003**, *15*, 763−775.
(9) Soler-Illia, G. J. D.; Sanchez, C.; Lebeau, B.; Patarin, J. *Chem. Rev.* **2002**, *102*, 4093−4138.
(10) Sanchez, C.; Soler-Illia, G.; Ribot, F.; Lalot, T.; Mayer, C. R.; Cabuil, V. *Chem. Mater.* **2001**, *13*, 3061−3083.
(11) Ying, J. Y.; Mehnert, C. P.; Wong, M. S. *Angew. Chem., Int. Ed.* **1999**, *38*, 56−77.
(12) Schuth, F.; Schmidt, W. *Adv. Mater.* **2002**, *14*, 629−638.
(13) Fan, H. Y.; Bentley, H. R.; Kathan, K. R.; Clem, P.; Lu, Y. F.; Brinker, C. J. *J. Non-Cryst. Solids* **2001**, *285*, 79−83.
(14) Schmidt, M.; Boettger, G.; Eich, M.; Morgenroth, W.; Huebner, U.; Boucher, R.; Meyer, H. G.; Konjhodzic, D.; Bretinger, H.; Marlow, F. *Appl. Phys. Lett.* **2004**, *85*, 16−18.
(15) Konjhodzic, D.; Bretinger, H.; Wilczok, U.; Dreier, A.; Ladenburger, A.; Schmidt, M.; Eich, M.; Marlow, F. *Appl. Phys. A* **2005**, *81*, 425−432.
(16) Falcaro, P.; Grosso, D.; Amenitsch, H.; Innocenzi, P. *J. Phys. Chem. B* **2004**, *108*, 10942−10948.
(17) Urade, V. N.; Hillhouse, H. W. *J. Phys. Chem. B* **2005**, *109*, 10538−10541.
(18) Luo, H. M.; Wang, D. H.; He, J. B.; Lu, Y. F. *J. Phys. Chem. B* **2005**, *109*, 1919−1922.
(19) Liu, N. G.; Dunphy, D. R.; Atanassov, P.; Bunge, S. D.; Chen, Z.; Lopez, G. P.; Boyle, T. J.; Brinker, C. J. *Nano Lett.* **2004**, *4*, 551−554.
(20) Hou, K.; Tian, B. Z.; Li, F. Y.; Bian, Z. Q.; Zhao, D. Y.; Huang, C. H. *J. Mater. Chem.* **2005**, *15*, 2414−2420.
(21) Hillhouse, H. W.; Tuominen, M. T. *Microporous Mesoporous Mater.* **2001**, *47*, 39−50.
(22) Li, A. P.; Muller, F.; Birner, A.; Nielsch, K.; Gosele, U. *J. Appl. Phys.* **1998**, *84*, 6023−6026.
(23) Thurn-Albrecht, T.; Steiner, R.; DeRouchey, J.; Stafford, C. M.; Huang, E.; Bal, M.; Tuominen, M.; Hawker, C. J.; Russell, T. *Adv. Mater.* **2000**, *12*, 787−791.

10.1021/cm0520766 CCC: $33.50
Published on Web 01/05/2006

ongoing and grand challenges in the field of self-assembled nanostructured thin films is to control phase topology, order, orientation, and composition.

Our understanding of the molecular, colloidal, and self-assembly processes that are involved in the coating and film formation process has evolved[25−27] significantly since the first reports of well-ordered thin films.[28−31] In an important development, Zhao and co-workers showed[32,33] that highly ordered two-dimensional hexagonal phase and "cubic" phase nanoporous thin films could be templated by nonionic triblock copolymers composed of poly(ethylene oxide)-poly(propylene oxide)-poly(ethylene oxide) blocks (PEO−PPO−PEO). Subsequently, it was shown[34] by Alberius and co-workers that the binary water/surfactant phase diagram could be used to predict the phase of the nanostructured inorganic/surfactant assembly. By using these calculations, the concentrations of the coating solution may be chosen rationally to narrow down the range of the synthesis parameters. However, it has been shown that the concentration of the silica and surfactant in the coating solution does not completely determine the ultimate nanostructure of the resulting film. Soler-Illia and co-workers demonstrated that the curvature of the hydrophilic/hydrophobic interface (and consequently the final nanophase) is also affected by the concentration of water in the initial coating solution.[35] This is a result of the fact that the rate of water evaporation from the film may be on the same time scale as the rate of silica condensation. This effect of the two competing processes on the ultimate nanostructure has been demonstrated directly by controlling the rate of evaporation (through control of relative humidity, RH) during and after the dipping process.[36,37] However, in addition to these kinetics effects, there is an equilibrium quantity of water that remains in the film that depends on the humidity (more specifically the chemical potential of water in the vapor phase).[38] This water content will also affect the final nanostructure if the condensation reaction is slower than the drying of the films. Further, the humidity can also affect orientation and order in the film. The systematic changes in order, orientation, and nanostructure in dip-coated films in response to humidity were recently demonstrated[39] by Tate and co-workers. In that paper it was shown that while a given nanostructure (two-dimensional hexagonal, rhombohedral, etc.) could be synthesized over a range of Si/EO and humidity, the films at a higher Si/EO ratio always produced more oriented films.

As a result of rationally formulated compositions based on comparisons with binary solvent/surfactant phase diagrams, as well as a host of Edisonian experiments, many different phases and orientations of self-assembled nanostructured thin films have been synthesized by dip-coating or spin-coating, including (1) a two-dimensional hexagonal phase[31,40] with hexagonal plane group *p*6*mm* (which distorts to a rectangular plane group *c*2*mm* upon drying),[41] (2) a three-dimensional hexagonal phase[33,42,43] with space group $P6_3/mmc$, (3) a body-centered cubic (bcc) phase with space group $Im\bar{3}m$ (which distorts to an orthorhombic *Fmmm* space group upon drying),[16,44] (4) a primitive cubic phase with space group $Pm\bar{3}n$,[33] (5) body-centered tetragonal phase[45] with space group *I*4/*mmm*, and (6) a distorted cubic phase[46] based on space group $Ia\bar{3}d$.

Here we are interested in film morphologies that may be able to yield good accessibility to the pore system and the substrate. The two-dimensional hexagonal and $Ia\bar{3}d$ phases are appealing because by symmetry they have continuous pores. However, nanoporous films derived from two-dimensional hexagonal self-assemblies typically form with their pores oriented in the plane of the substrate. Ordered disclinations may yield domains of pores that are directed perpendicular to the substrate over limited regions,[47] but they are not open to the vapor phase. More recently, Rankin and Koganti have shown[48] that confining as-synthesized films between two coated substrates may yield two-dimensional hexagonal films with domains where the pores are perpendicular to the substrate. Another promising approach to forming nanoporous thin films with good accessibility to the pore structure and underlying substrate is the use of bicontinuous cubic phases (space group *Ia*3*d*) to yield films with

(24) Kim, S. H.; Misner, M. J.; Xu, T.; Kimura, M.; Russell, T. P. *Adv. Mater.* **2004**, *16*, 226.
(25) Brinker, C. J.; Lu, Y. F.; Sellinger, A.; Fan, H. Y. *Adv. Mater.* **1999**, *11*, 579.
(26) Grosso, D.; Cagnol, F.; Soler-Illia, G.; Crepaldi, E. L.; Amenitsch, H.; Brunet-Bruneau, A.; Bourgeois, A.; Sanchez, C. *Adv. Funct. Mater.* **2004**, *14*, 309−322.
(27) Doshi, D. A.; Gibaud, A.; Goletto, V.; Lu, M. C.; Gerung, H.; Ocko, B.; Han, S. M.; Brinker, C. J. *J. Am. Chem. Soc.* **2003**, *125*, 11646−11655.
(28) Yang, H.; Kuperman, A.; Coombs, N.; Mamiche-Afara, S.; Ozin, G. A. *Nature* **1996**, *379*, 703−705.
(29) Hillhouse, H. W.; Okubo, T.; van Egmond, J. W.; Tsapatsis, M. *Chem. Mater.* **1997**, *9*, 1505−1507.
(30) Trau, M.; Yao, N.; Kim, E.; Xia, Y.; Whitesides, G. M.; Aksay, I. A. *Nature* **1997**, *390*, 674−676.
(31) Lu, Y. F.; Ganguli, R.; Drewien, C. A.; Anderson, M. T.; Brinker, C. J.; Gong, W. L.; Guo, Y. X.; Soyez, H.; Dunn, B.; Huang, M. H.; Zink, J. I. *Nature* **1997**, *389*, 364−368.
(32) Zhao, D.; Yang, P.; Melosh, N.; Feng, J.; Chmelka, B. F.; Stucky, G. D. *Adv. Mater.* **1998**, *10*, 1380.
(33) Zhao, D. Y.; Yang, P. D.; Margolese, D. I.; Chmelka, B. F.; Stucky, G. D. *Chem. Commun.* **1998**, 2499−2500.
(34) Alberius, P. C. A.; Frindell, K. L.; Hayward, R. C.; Kramer, E. J.; Stucky, G. D.; Chmelka, B. F. *Chem. Mater.* **2002**, *14*, 3284−3294.
(35) Soler-Illia, G.; Crepaldi, E. L.; Grosso, D.; Durand, D.; Sanchez, C. *Chem. Commun.* **2002**, 2298−2299.
(36) Gibaud, A.; Grosso, D.; Smarsly, B.; Baptiste, A.; Bardeau, J. F.; Babonneau, F.; Doshi, D. A.; Chen, Z.; Brinker, C. J.; Sanchez, C. *J. Phys. Chem. B* **2003**, *107*, 6114−6118.
(37) Cagnol, F.; Grosso, D.; Soler-Illia, G.; Crepaldi, E. L.; Babonneau, F.; Amenitsch, H.; Sanchez, C. *J. Mater. Chem.* **2003**, *13*, 61−66.
(38) Gu, Z. Y.; Alexandridis, P. *J. Pharm. Sci.* **2004**, *93*, 1454−1470.
(39) Tate, M. P.; Eggiman, B. W.; Kowalski, J. D.; Hillhouse, H. W. *Langmuir* **2005**, *21*, 10112−10118.
(40) Zhao, D. Y.; Feng, J. L.; Huo, Q. S.; Melosh, N.; Fredrickson, G. H.; Chmelka, B. F.; Stucky, G. D. *Science* **1998**, *279*, 548−552.
(41) Klotz, M.; Albouy, P. A.; Ayral, A.; Menager, C.; Grosso, D.; Van der Lee, A.; Cabuil, V.; Babonneau, F.; Guizard, C. *Chem. Mater.* **2000**, *12*, 1721−1728.
(42) Besson, S.; Ricolleau, C.; Gacoin, T.; Jacquiod, C.; Boilot, J. P. *J. Phys. Chem. B* **2000**, *104*, 12095−12097.
(43) Grosso, D.; Balkenende, A. R.; Albouy, P. A.; Lavergne, M.; Mazerolles, L.; Babonneau, F. *J. Mater. Chem.* **2000**, *10*, 2085−2089.
(44) Besson, S.; Ricolleau, C.; Gacoin, T.; Jacquiod, C.; Boilot, J. P. *Microporous Mesoporous Mater.* **2003**, *60*, 43−49.
(45) Falcaro, P.; Costacurta, S.; Mattei, G.; Amenitsch, H.; Marcelli, A.; Guidi, M. C.; Piccinini, M.; Nucara, A.; Malfatti, L.; Kidchob, T.; Innocenzi, P. *J. Am. Chem. Soc.* **2005**, *127*, 3838−3846.
(46) Hayward, R. C.; Alberius, P. C. A.; Kramer, E. J.; Chmelka, B. F. *Langmuir* **2004**, *20*, 5998−6004.
(47) Hillhouse, H. W.; van Egmond, J. W.; Tsapatsis, M.; Hanson, J. C.; Larese, J. Z. *Chem. Mater.* **2000**, *12*, 2888−2893.
(48) Koganti, V. R.; Rankin, S. E. *J. Phys. Chem. B* **2005**, *109*, 3279−3283.

an interconnected pore network.[46] The benefit with this approach is that orientation of the film is not an issue. However, films of these phases have been challenging to synthesize, typically exist over very extremely small ranges of composition and temperature, and may coexist with other phases.[46]

An alternative approach to synthesize films with good pore accessibility is to form cagelike structures that are interconnected by windows or microporosity. Self-assembly of spherical or elliptical micelles typically yields structures with spherical or elliptical voids. For powders it has been shown through electron crystallography and adsorption studies that in many cases these voids are connected by openings that yield a continuous pore structure.[49,50] Note that, for powders synthesized with PEO−PPO−PEO triblock copolymers templates, the voids may be interconnected by microporosity[51] independent of any larger mesoscale openings between voids. Matos and co-workers[52] and Kleitz and co-workers[53] later showed that the apertures could be controlled and systematically expanded by hydrothermal treatment. For structures templated by Pluronic F127 ($PEO_{106}-PPO_{70}-PEO_{106}$), it was later shown that the pore apertures could be tuned by hydrothermal treatments from ~0.4 nm for treatments at low temperatures or short times up to 5 nm for treatments of 100 °C for 3 days.

However, using these techniques to adjust the pore aperture for thin films presents a challenge. Films are typically synthesized at room temperature and thus are expected to have poor connectivity between voids. However, despite the growing body of work on powders, there are no detailed structural studies on connectivity in films. After film formation by dip-coating or spin-coating, the silica in the film is quite poorly condensed. This may lead to problems with dissolution, cracking, and adhesion if the films are immersed in solution for hydrothermal treatment. Tailoring these apertures or interconnections between voids then becomes a key issue in engineering these films. One challenge is that the cubic phase films are typically formed with surfactants with large headgroups such as Pluronic F127 ($PEO_{106}-PPO_{70}-PEO_{106}$). The high PEO/PPO ratio yields high curvature at the PEO−PPO interface and thus forms spherical micelles. However, this also makes forming interconnections between cages more difficult at room temperature because the cage to cage distance should scale with PEO length. In this study, we investigate the synthesis of high curvature phases with smaller PEO segments using Pluronic P123 ($PEO_{20}-PPO_{70}-PEO_{20}$). There is little information in the literature on P123 templated films with high curvature mesophases (e.g., cubic structures), and the structure reported here differs from that previously reported by Alberius et al.[34] Here, we report the synthesis and structure of highly ordered and oriented self-assembled films with a rhombohedral structure. Detailed studies of the phase diagram including the effects of humidity on orientation and order[39] and studies on the accessibility of the films by analyzing carbon replicas[54] are reported separately.

2. Experimental Section

Film Synthesis. Films were synthesized on a variety of substrates (covering a wide range of hydrophilicity) including borosilicate glass, quartz, gold-coated glass, silicon, and F-doped tin oxide, each yielding similar results. Data presented in this report are from borosilicate glass "cover slide" substrates (60 mm × 22 mm × 0.18 mm) purchased from VWR Scientific and cleaned in a 1 wt % Alconox solution at 65 °C for 30 s. The substrates were then rinsed with dionized ultrafiltrated water and air-dried thoroughly prior to dip-coating. After cleaning, scotch tape was applied to one side of the substrate to prevent film formation on that side. The scotch tape was removed prior to X-ray scattering and calcination. The presence of the tape had no effect on the film formation on the opposite side as determined by X-ray scattering from films prepared without using tape.

The dip-coating solution was prepared using a mixture of P123 obtained from BASF and ACS reagent grade tetraethyl orthosilicate (TEOS), ethanol (EtOH), and hydrochloric acid (HCl) obtained from Aldrich. All reagents were used as received. Twenty-four hours prior to dip-coating, a surfactant precursor solution was prepared and allowed to equilibrate by adding 2.99 g of P123 and 12.84 g of EtOH to a sealed high-density polypropylene (HDPE) bottle and stirred at room temperature (~21 °C). The silica precursor solution was prepared by adding 9.48 g of dilute HCl/water (pH = 1.78) to 19.19 g of EtOH in a HDPE bottle. Then, 18.22 g of TEOS was added. The solution was sealed and stirred vigorously for exactly 20 min, at which time the surfactant precursor was added to the silica precursor. The combined solution was resealed and stirred in a water bath at 5 °C for exactly 10 min. The final molar composition of the dip-coating solution was 0.00595:1:0.002:6.01:7.95 P123/TEOS/HCl/H_2O/EtOH. The dip-coating solution was then immediately poured into a small glass beaker and filled to within 1 mm of the top before being placed in a humidity-controlled dip-coating chamber. The humidity inside the chamber was controlled by a forced flow mixture of dry and saturated air streams to 60 ± 2% RH. The humid air inlet was directed away from the film coating location so as to minimize the effects of forced convection on the coating process. The beakers were filled to the rim so that the humidity above the film during dipping is as close as possible to the humidity of the bulk air in the chamber. After dipping at a speed of 1 mm/s, films were left for 2 min in the dipping chamber before being rapidly transferred to the second humidity-controlled chamber (also at 60% RH) where they were aged for 12 h. Films were then calcined at 400 °C for 4 h with heating and cooling ramps of 1 °C/min.

Electron Microscopy. Plan-view micrographs of calcined films were recorded using a Hitachi S-4800 high-resolution field emission scanning electron microscope (FESEM). The working distance was 8.1 mm, and the accelerating voltage was 3.0 kV. Each sample received a layer of carbon paint around the edges of the substrate to reduce charging effects of the mesoporous silica film.

X-ray Scattering. As-synthesized and calcined films were characterized by grazing-incidence small-angle X-ray scattering

(49) Sakamoto, Y.; Kaneda, M.; Terasaki, O.; Zhao, D. Y.; Kim, J. M.; Stucky, G.; Shim, H. J.; Ryoo, R. *Nature* **2000**, *408*, 449−453.
(50) Sakamoto, Y.; Diaz, I.; Terasaki, O.; Zhao, D. Y.; Perez-Pariente, J.; Kim, J. M.; Stucky, G. D. *J. Phys. Chem. B* **2002**, *106*, 3118−3123.
(51) Imperor-Clerc, M.; Davidson, P.; Davidson, A. *J. Am. Chem. Soc.* **2000**, *122*, 11925−11933.
(52) Matos, J. R.; Kruk, M.; Mercuri, L. P.; Jaroniec, M.; Zhao, L.; Kamiyama, T.; Terasaki, O.; Pinnavaia, T. J.; Liu, Y. *J. Am. Chem. Soc.* **2003**, *125*, 821−829.
(53) Kleitz, F.; Liu, D. N.; Anilkumar, G. M.; Park, I. S.; Solovyov, L. A.; Shmakov, A. N.; Ryoo, R. *J. Phys. Chem. B* **2003**, *107*, 14296−14300.
(54) Eggiman, B. W.; Owens, D.; Urade, V. N.; Hillhouse, H. W. **2005**, submitted.

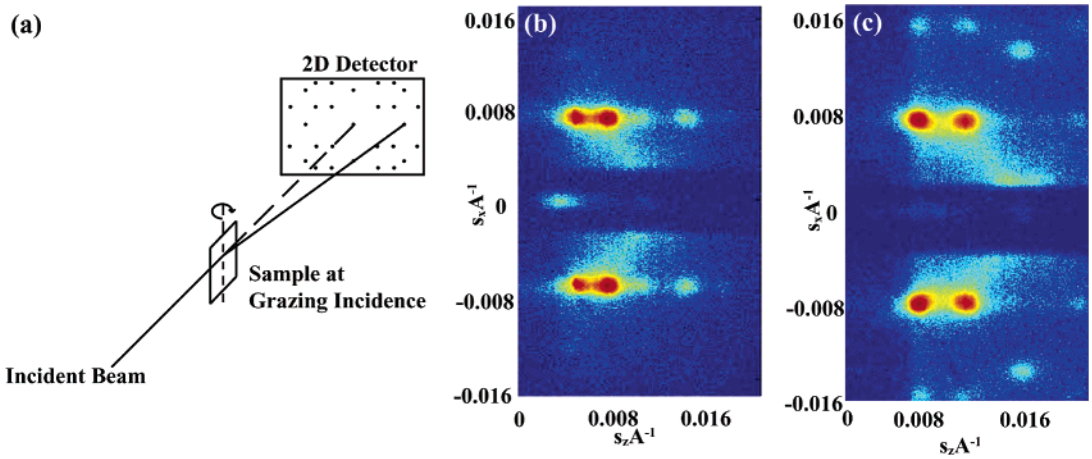

Figure 1. (a) Experimental geometry used to collect GISAXS patterns of (b) an as-synthesized and (c) a calcined $R\bar{3}m$ nanostructured silica thin film. The intensity on the left side of the two-dimensional pattern is below the horizon of the substrate, and, therefore, only $s_z > 0$ is shown in the figure. In addition, a beam stop was added along $s_x = 0$ to prevent damage to the detector from the specular beam.

(GISAXS) using a three-pinhole SAXS camera (Molecular Metrology) with a microfocus X-ray source, an Osmic MaxFlux confocal X-ray optic, and a gas-filled two-dimensional multiwire detector at a camera length of 1424 mm. Samples were mounted on custom-made two-axis goniometer in which samples are free to rotate 180° about the vertical axis (see Figure 1a). The detector was calibrated using a silver behenate powder standard. The specular beam intensity was attenuated along the x axis with aluminum strips. These strips block reciprocal space in a region from -0.002 Å^{-1} $< s_x <$ 0.002 Å^{-1} and from 0.0 Å^{-1} $< s_z <$ 0.020 Å^{-1}. The intensities in each two-dimensional scattering pattern are displayed on a log scale for illustrative purposes.

X-ray Spot Pattern Simulation. The measured scattering patterns were analyzed using NANOCELL.[55] This code uses kinematic theory and the distorted-wave Born approximation to model the Bragg peak positions, peaks from the specular beam, and artifacts arising from the refraction/reflection events in two-dimensional GISAXS geometry for any given unit cell and model of disorder. Simulated patterns were matched and overlaid on measured data to elucidate the structure, orientation, and disorder in the samples. Samples may have a single orientation with respect to the substrate, freedom to rotate about the substrate normal, or complete rotational freedom (powderlike pattern). Details about NANOCELL may be found at http://www.ecn.purdue.edu/~hugh.

3. Results and Discussion

The range of synthesis compositions investigated was chosen by employing the method developed by Alberius et al.[34] In this method, the silica content of the dipping solution is selected such that the volume fraction of the silica in the nanostructure is roughly equal to the volume fraction of water in the desired region of the binary phase diagram. The binary phase diagram of P123 with water reported by Wanka et al. shows a cubic lyotropic liquid crystal region at 22−38 vol % P123 in water.[56] However, Holmqvist et al. report the cubic region only from 29−32 vol % P123.[57] To estimate the Si/EO ratio needed in the dipping solution, one needs to estimate the density of the silica part of the self-assembled nanostructure. For calculation purposes, it is assumed that the silica exists as $Si(OH)_4$ in the self-assembled film. Upon condensation, 1 mol of $Si(OH)_4$ would yield 1 mol of SiO_2 plus 2 mol of H_2O. Thus, the density of $Si(OH)_4$ is estimated by the density of one SiO_2 and two H_2O. Under this assumption, Si/EO ratios of 7.86−3.70 and 5.47−4.84 in the coating solution will correspond to the volume percent ranges reported by Wanka et al. and Holmqvist et al., respectively. In the present work, the ordered and oriented structures described below were synthesized at Si/EO > 3.97 and at moderate RH (40−60% RH). GISAXS patterns of the as-synthesized and calcined films are shown in Figure 1. Much information can be gleaned from these data. First, we concluded that the films are highly ordered as a result of the large number of well-resolved diffraction peaks. In principle these could exist from multiple phases, but below we show that this is in fact not the case and that these patterns arise from a single phase. Second, because of the fact that we see distinct spots, we conclude that the films are highly oriented (relative to the plane of the substrate) all the way though the thickness of the film. If the films were not oriented at intermediate depths, we would observe rings in the GISAXS pattern. Also, we note that the as-synthesized and calcined GISAXS patterns are qualitatively similar, but in the calcined film, the peaks are shifted to a higher scattering vector and are more intense as a result of the enhanced contrast in electron density from the removal of the template. Upon attempts to index these films, they could not be indexed with any orientation from any cubic space group.

To probe a broader range of reciprocal space, a calcined film synthesized on a 150 μm thick silica cover slide was examined in low-angle transmission SAXS at a range of incident angles from near grazing-angle up until the incidence beam was perpendicular to the substrate. The data are shown in Figure 2 after correcting for changes in the transmission factor as a function of apparent thickness of the substrate at a given angle of incidence. The peak along the $s_x = 0$ line (the peak that would be observed in a normal powder X-ray diffractometer) disappears with increasing grazing angle while spots at $s_z < 0$ and $s_z > 0$ shift toward $s_x = 0$ along

(55) Tate, M. P.; Urade, V. N.; Kowalski, J. D.; Wei, T. C.; Hamilton, B. D.; Eggiman, B. W.; Hillhouse, H. W. **2005**, submitted.
(56) Wanka, G.; Hoffmann, H.; Ulbricht, W. *Marcomolecules* **1994**, *27*, 4145−4159.
(57) Holmqvist, P.; Alexandridis, P.; Lindman, B. *J. Phys. Chem. B* **1998**, *102*, 1149−1158.

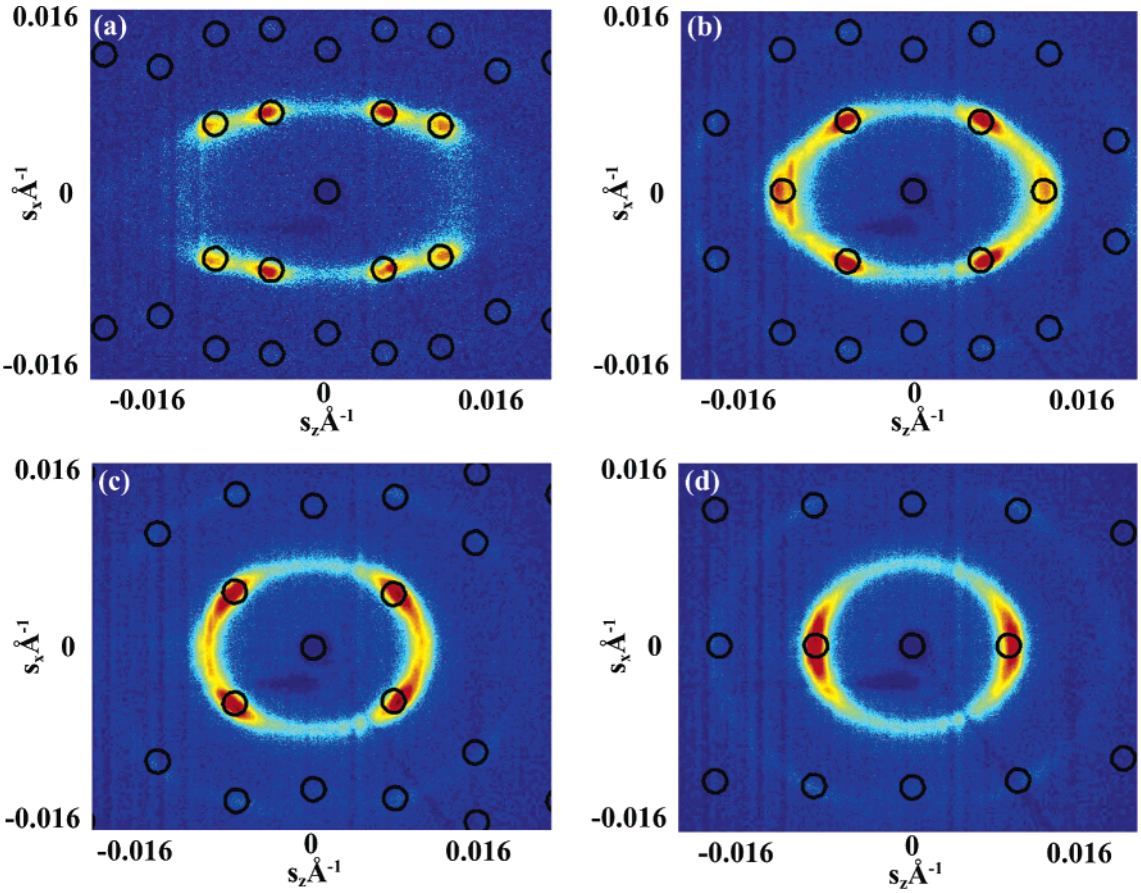

Figure 2. Transmission SAXS data and NANOCELL simulation overlays for the following angles of incidence: (a) 25, (b) 40, (c) 50, and (d) 60°. The intensity of each pattern was normalized to account for the changes in attenuation of the incident beam due to the change in thickness of the substrate along the flight path of the incident beam as the sample is rotated. Note that the slight asymmetry in the predicted peak positions at higher angles is real and due to the curvature of the Ewald sphere.

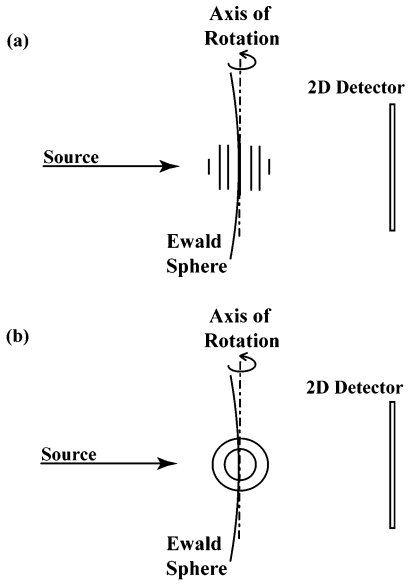

Figure 3. Sketch of the ring structure of reciprocal space for (a) the case when the substrate normal is parallel to the incident beam (transmission SAXS) and (b) the case when the substrate normal is perpendicular to the beam (GISAXS). For case b, spots will appear on the detector at every location the ring crosses the Ewald sphere. Note that in case a if any ring is present at $s_z = 0$, it would appear as a ring on the detector.

an arc. Analysis of this pattern of how the Bragg spots shift confirms that reciprocal space consists of rings (Figure 3). Thus, each quadrant of the GISAXS pattern is populated by spots where the Ewald sphere slices through each ring. This structure of reciprocal space is produced by a film that is highly oriented in the plane of the substrate but possesses many rotational orientations within the plane. This type of disorder had been previously noted[9,41,46,58] in other nanostructured films to fit GISAXS patterns. However, the rotation data shown in Figure 2 is the first direct observation of the ringlike structures in reciprocal space produced by these self-assembled nanostructured films.

The structure and orientation is further elucidated in high-resolution top-view FESEM images. Here, a highly ordered pattern of pores is observed with nearly perfect sixfold symmetry, Figure 4. Because the GISAXS data show that the film is oriented all the way through the thickness, the FESEM data limits the possible set of space groups and orientations to those that display sixfold or threefold axes perpendicular to the substrate. These include all cubic and rhombohedral space groups with (111) orientation and hexagonal space groups with (001) orientation. NANOCELL[55] was used to simulate the GISAXS patterns of all these space groups. Several of the simulations are shown in Figure 5. It is observed that despite the different extinction rules for the various cubic space groups, the simulated $Im\bar{3}m$, $Fm\bar{3}m$, and $Pm\bar{3}n$ patterns are qualitatively similar to each other as well as the observed GISAXS pattern. However, none of these space groups can quantitatively match the

(58) Crepaldi, E. L.; Soler-Illia, G.; Grosso, D.; Cagnol, F.; Ribot, F.; Sanchez, C. *J. Am. Chem. Soc.* **2003**, *125*, 9770−9786.

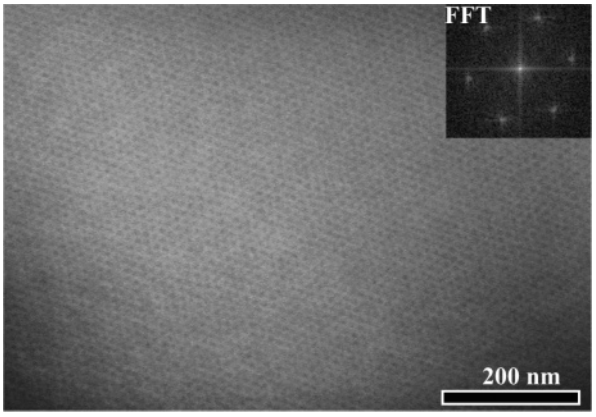

Figure 4. Top-view FESEM image of the nanostructured film clearly showing a sixfold symmetry axis that is perpendicular to the substrate. This limits the possible structures to the (111) oriented cubic or rhombohedral space groups and (001) oriented hexagonal space groups.

observed spot pattern. Both the body-centered Bravias lattice (I) as well as the face-centered Bravais lattice (F) can be described by rhombohedral primitive lattices with $a_R = 0.866a_I$ and $\alpha_R = 109.47°$ and $a_R = 0.707a_F$ and $\alpha_R = 60°$, respectively. In addition, a primitive cubic lattice can also be considered as a primitive rhombohedral lattice ($a_R = a_P$, $\alpha_R = 90°$). The rhombohedral space group $R\bar{3}m$ is a maximal nonisomorphic subgroup of $Im\bar{3}m$, $Fm\bar{3}m$, $Pm\bar{3}m$, and $Pn\bar{3}m$, while the rhombohedral space group $R\bar{3}c$ is a maximal nonisomorphic subgroup of $Pm\bar{3}n$ and $Ia\bar{3}d$. Also, in each of the cubic lattices, the [111] direction is coincident with the [111] direction in the rhombohedral cell. Thus, NANOCELL was used to simulate the spot patterns of (111) oriented $R\bar{3}m$ and $R\bar{3}c$ space groups with rotational freedom about the [111] axis. It is found that the experimental data may be accurately fit with lattice constants $a = 112$ Å and $\alpha = 86°$) in the $R\bar{3}m$ space group, as shown in Figure 6. In addition these lattice constants quantitatively fit the spot positions in the rotation data shown in Figure 2.

While the $R\bar{3}m$ space group accurately describes the main features of reciprocal space of the nanostructured film, it is unlikely that the film self-assembles directly into this lower symmetry space group. Likely, a higher symmetry cubic space group is present early on in the coating process that distorts under the uniaxial contraction that occurs upon drying. First, we note from above that several cubic space groups can be described by a primitive rhombohedral unit cell and that each cubic Bravais lattice type (F, P, or I) corresponds to a rhombohedral cell with specific values of the angle α (60, 90, and 109.47°, respectively). These different starting structures are illustrated in Figure 7 along with the location of the equivalent rhombohedral lattice vectors for each possible parent structure. Next, we note that if the unit cell is (111) oriented, then upon contraction (a decrease in the d_{111} spacing) the angle α must increase. This can be most easily understood by visual inspection of the unit cell (see Figure 7) but can be verified from the d spacing formula for the (111):

$$d_{111}^{\text{rhombohedral}} = \sqrt{\frac{a^2(1 - 3\cos^2\alpha + 2\cos^3\alpha)}{3\sin^2\alpha + 6\cos^2\alpha - 6\cos\alpha}}$$

Given that the fitted value of α is 86°, if the unit cell was cubic before contraction, it must have been a face-centered

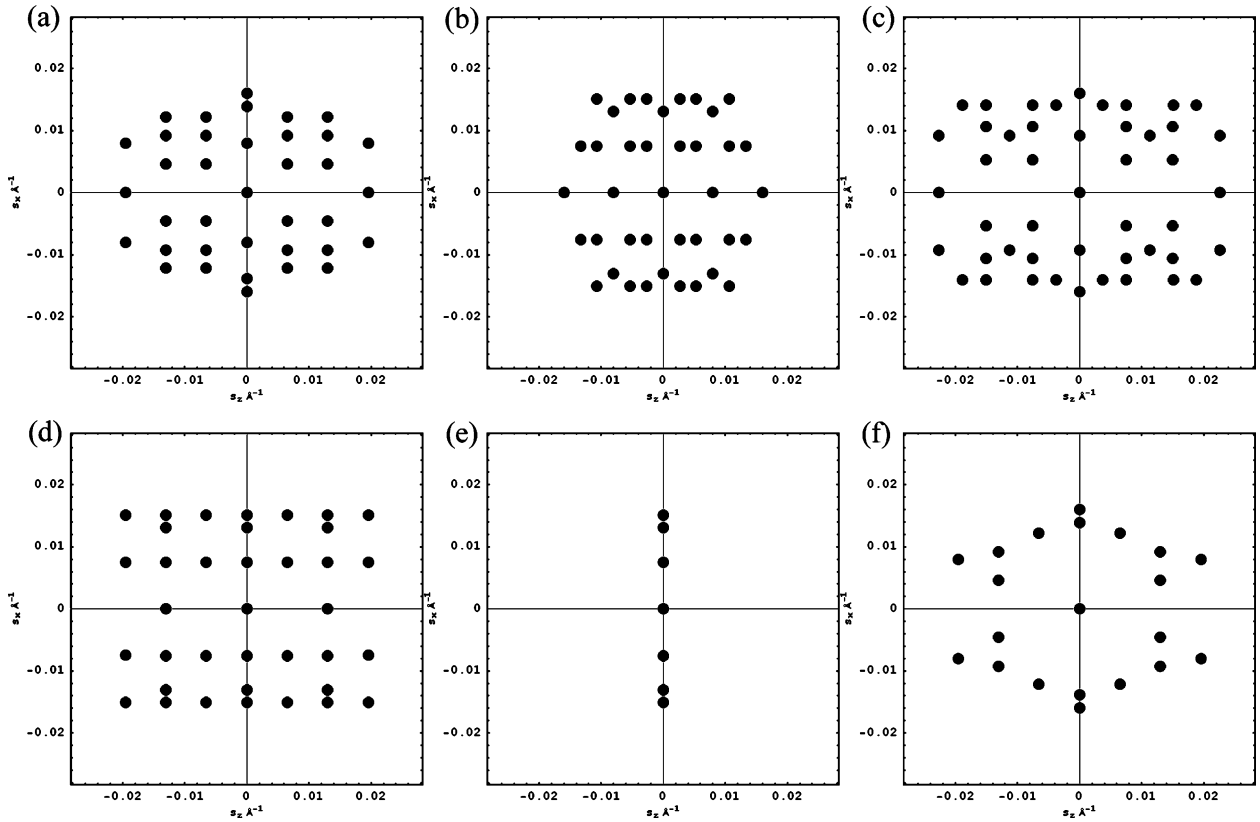

Figure 5. NANOCELL simulations of (a) (111) oriented $Im\bar{3}m$, (b) (111) oriented $Fm\bar{3}m$, (c) (111) oriented $Pm\bar{3}n$, (d) (001) oriented $P6_3/mmc$, (e) two-dimensional hexagonal $p6mm$ with sixfold axis perpendicular to the substrate, and (f) (111) oriented $Ia\bar{3}d$ nanostructured thin films. The nearest neighbor spacing (150 Å for simulation purposes) was kept constant to more closely mimic the physical situation, as opposed to keeping the lattice constant the same,

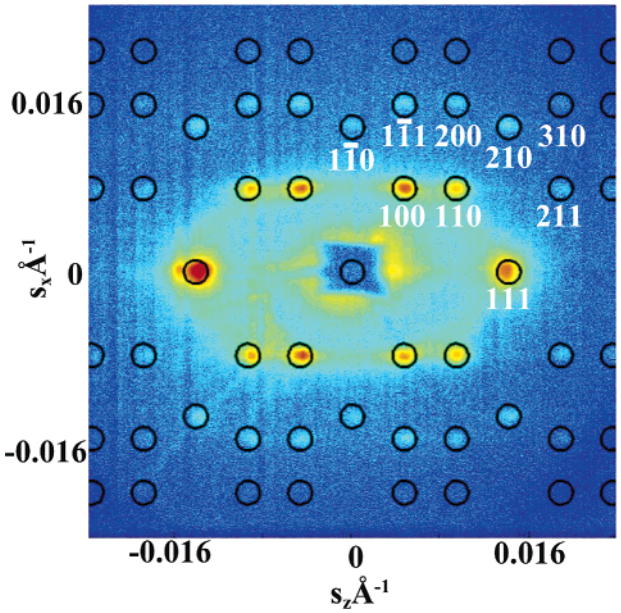

Figure 6. NANOCELL simulation of a (111) oriented $R\bar{3}m$ structure (a = 112 Å, α = 86°) overlaid onto the low-angle (2.25°) transmission SAXS pattern of the calcined nanostructured thin film on a cover slide substrate. The film is placed on the detector side of the substrate.

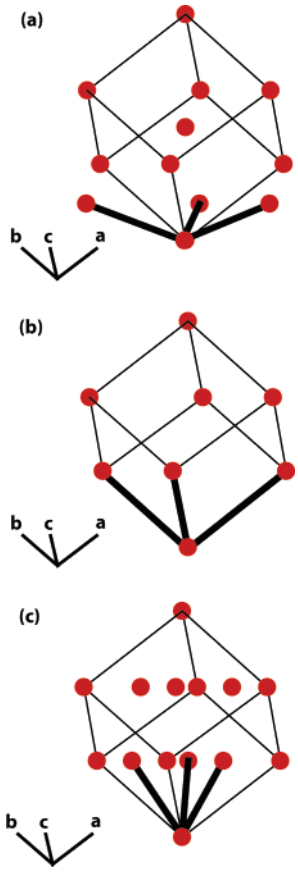

Figure 7. Each (a) I, (b) P, and (c) F (111) oriented cubic space group may be described by an equivalent rhombohedral primitive cell (R). For the I cell, the lattice vectors of the R cell (illustrated by the thick black lines) point from a unit cell corner to the body centers of three adjacent unit cells. For the P cell, the R lattice vectors are the same as the P cell. Finally, for the F cell, the R lattice vectors point from the corner of the unit cell to three face centers on the unit cell. Note: The red dots indicate only the location of the lattice points and do not represent any information about pore structure or connectivity.

cubic (fcc) lattice. Thus, the fitted $R\bar{3}m$ lattice constants suggest that, upon the initial assembly, the nanostructure is a face-centered lattice, likely an $Fm\bar{3}m$ cubic close packing of micellar aggregates.

Additionally, in the fcc structure the (111) plane has the highest planar density of micelles. Thus, if there is a favorable interaction between the PEO/silica and the substrate, fcc films should be oriented with the (111) parallel to the substrate. Because the [111] direction in the fcc structure is perpendicular to the (111) plane and is the same direction as the [111] direction in the rhombohedral films, the resulting contracted rhombohedral films should also be (111) oriented. If the parent phase of the rhombohedral structure is a fcc structure, this opens the possibility that the film may contain ABAB stacking sequences in addition to the ABCABC stacking sequence of a perfect fcc structure. If these ABAB sequences existed in any significant quantity, one would observe scattered intensity along the $s_x = 0$ plane in the low-angle transmission SAXS data at s_z values corresponding to the shorter spacing from the ABAB sequence as compared to the ABCABC sequence. As can be seen in Figure 6, no intensity is observed at s_z values larger than the (111) Bragg peak of the $R3m$ phase. On the basis of this, we conclude that the stacking sequence of the parent fcc phase is primarily ABCABC.

4. Conclusions

Highly ordered rhombohedral phase mesoporous silica films have been synthesized and characterized by GISAXS. The films are highly oriented with the (111) planes orientated parallel to the substrate. It is conjectured that the rhombohedral structure results from the contraction of a face-centered lattice. If this conjecture is true, it would explain the observed orientation of the rhombohedral films.

In self-assembling block copolymer/solvent systems, it has been previously shown[59] that the micelle interaction potential dictates how the micelles pack together, with longer range interactions yielding bcc packing as opposed to fcc. This has been observed systematically in both polystyrene−polysiopropene in decane systems[59] and poly(ethylene oxide)−poly(butylene oxide) in water systems.[60] The observation of fcc packing here may yield clues as to the conformation of the corona and the effect the silica has on the micelle−micelle interactions. One may expect to see fcc−bcc transitions depending on the oligomeric structure and concentration of silica.

The close packing arrangement reported here may yield better intercage connections than a body-centered packing. It is also noted that, as a result of the uniaxial contraction, the window formation and pore topology could differ significantly from face-centered powder samples. While pore connectivity cannot be determined from the data presented above, stable carbon replicas of the films have been synthesized,[54] which demonstrates that the pore structure is at least interconnected by microporosity.

Acknowledgment. The authors wish to acknowledge financial support from National Science Foundation under the

(59) McConnell, G. A.; Gast, A. P.; Huang, J. S.; Smith, S. D. *Phys. Rev. Lett.* **1993**, *71*, 2102−2105.
(60) Hamley, I. W.; Daniel, C.; Mingvanish, W.; Mai, S. M.; Booth, C.; Messe, L.; Ryan, A. J. *Langmuir* **2000**, *16*, 2508−2514.

CAREER Award (0134255-CTS) and the Purdue Research Foundation (PRF-6904009). In addition, the NSF funded (MRI program award 0321118-CTS) facility for In-situ X-ray Scattering from Nanomaterials and Catalysts was used to collect GISAXS data. Additionally, the authors would like to thank the Purdue Electron Microscopy Center at the School of Materials Engineering, Purdue University, for FESEM usage and BASF for providing the triblock copolymer templates.

CM0520766